Design Optimization for the Performance Enhancement of Large Scale Thermosyphons

B. H. Kim* and C. J. Kim**

(Received August 18, 1994)

As a method to enhance performance of a low-tilt thermosyphon, a groove wick was recommended and individual performance limitations which includes the capillary, boiling, entrainment, viscous and sonic limits corresponding to the existing wick configuration were first examined for different operating vapor temperatures using conventional steady-state techniques available in the literature.

Second, using a computer model developed to predict the axial liquid pressure drop and the boiling limit heat flux, a parametric investigation was performed to determine an optimal configuration of groove wicks designed to improve the operational performance. Results of the present study showed that the heat transport capacity was significantly affected by wick geometry, such as groove angle, groove width and groove depth.

Key Words: Thermosyphon, Capillary Pressure, Limitation Wick, Groove, Optimization

Nomenclature

A : area of flow passage(m^2)
A_w : wick cross-sectional area (m^2)
d_g : opening width of a groove wick (m)
$d_{h,w}$: hydraulic diameter of a wick pore (m)
d_i : inner wall diameter (m)
d_v : vapor core diameter (m)
D_v : dynamic pressure coefficient
f_v : liquid and vapor friction factor at the interface
f_l : drag coefficient for liquid flow
F_l : liquid frictional coefficient
F_v : vapor frictional coefficient
h_{fg} : latent heat of vaporization (J/kg)
k_{eff} : effective thermal conductivity (W/(m.K))
k : thermal conductivity (W/(m.K))
K_l : permeability of wick (m^2)
L_{eff} : effective length of a heat pipe (m)
Ma_v : Mach number
M : molecular weight (kg/kmol)
N_{vi} : dimensionless viscosity number
ΔP_{cm} : maximum capillary pressure (Pa)
ΔP : pressure drop (Pa)
q : transport (W)
q'' : heat transport per unit cross-sectional area (W/m^2)
r_c : capillary radius (m)
r_i : inner radius of a thermosyphon (m)
$r_{h,l}$: hydraulic radius of liquid channel (m)
r_n : nucleation radius (m)
r_v : vapor core radius (m)
$\bar{R}$: universal gas constant (8.314 kJ/kmol K)
Re : Reynolds number of vapor flow
U_{vc} : critical mean velocity (m/s)
w : groove width (m)
w_f : groove fin width (m)

Greek Symbols

δ : groove depth (m)
γ : gas constant (J/(kg.K))
λ : wave-length (m)
ε : porosity of a wick
ψ : tilt angle (degree)
μ : viscosity of fluids (Pa. s)
ρ : density of fluids (kg/m^3)

*Samsung Electronics Co LTD(air conditioning division)
**Professor, Department of Mechanical Engineering in Sung Kyun Kwan University.

σ : surface tension of the liquid (N/m)
O : wetting angle (degree)

Subscripts

ad : adiabatic region
b : boiling limit
c : condenser or critical values at the onset of instability or entrainment
cap : capillary limit
cm : maximum capillary pressure
e : entrainment limit or evaporator
f : groove fin
l : liquid
n : normal capillary pressure
o : stagnation property
pm : effective capillary pressure
s : sonic limit
v : vapor
vi : viscous limit
w : wick material

1. Introduction

Thermosyphons have been widely utilized for energy recovery or air preheaters because they are very efficient heat transfer devices of high thermal conductance (Tien and Chung, 1979; Peterson and Bage, 1991). Here, the thermosyphons use gravitational hydrostatic head as the primary driving force and thus have no wick in most cases since there is no difference in the heat transport capacities between wicked and non-wicked ones at a high tilt. This might be true for small scale thermosyphons which show neither problems in vertical installation nor difficulties expected during the startup process.

However, for large scale types of thermosyphons, the vertical or high tilt installation is not recommended because of not only space limitations but also excessive overshooting of the evaporator liquid and wall temperatures. In order to resolve these problems, an axial and circumferential wick may be recommended (Busse and Kemme, 1980; Prenger and Kemme, 1981). The wick is designed to expedite the liquid flow from the condenser to the evaporator and as a result, high transport capacity could be obtained even at a small tilt. In addition, the wick may prevent earlier peripheral dry-out (due to entrainment), which leads to significant degradation in the performance and also could prevent overshooting of the liquid and wall temperatures by enhancing the heat transfer coefficient of normal pool boiling (Carey, 1992) that can be regarded as the most frequent boiling regime occurring in the evaporator during the startup of thermosyphons.

There are several methods by which the operational characteristics and performance limitations of the thermosyphons and heat pipes can be enhanced. This is particularly true for the long, large scale types of thermosyphons typically utilized for energy recovery or air preheaters. Among these methods, optimization of the axial/circumferential groove design or wicking structure may be the most important one even though evaluation of various pre-charge cleaning or surface enhancement technique developed for specific container, wicking structure, and working fluid combinations also affect the resultant performance of the thermosyphon (Dunn and Reay, 1982).

The overall objective of this investigation was to evaluate the existing ABB thermosyphon wicking design (ABB Air Preheater Inc., NY, USA) in an attempt to improve the operational characteristics and increase the performance limitations. This will be accomplished by optimizing the groove design. The resulting improvements in the operational characteristics and increases in the performance limits can then be implemented in order to reduce the total number of required thermosyphons or to reduce the angular tilt required for a specific application

2. Performance Limitations

In order to determine the optimal groove configuration of any heat pipe or thermosyphon, it is first necessary to determine the individual performance limitation. In the present study, these limits, which include the capillary, boiling, entrainment, viscous, and sonic limits were approximated using conventional steady-state techniques available in the literature (Chi, 1976;

Dunn and Reay, 1982; Ivanovskii et al., 1982). In the following, the procedure is first summarized for each limit and then the various limits are calculated and compared as a function of operating vapor temperature in the evaporator.

2.1 Capillary limitation

To determine the capillary limit (or dry-out limit), pressure drops in both liquid and vapor channels were investigated. A one-dimensional vapor flow model ($Ma_v < 0.2$) was introduced to predict the vapor pressure drop, while the momentum equation for the liquid flow was simplified and solved to calculate the liquid pressure drop by utilizing previous investigations for wick permeability (Chi, 1976).

The maximum heat transport capacity of a given heat pipe/thermosyphon configuration and orientation, illustrated in Fig. 1, can be determined using a one-dimension pressure balance model. Utilizing the technique presented by Chi (1976), this expression can be written as

$$\Delta P_{cm} - \Delta P_n - \Delta P_a = \int_0^{L_t} (F_l + F_v)\, q\, dx \quad (1)$$

where ΔP_{cm} is the maximum capillary pressure and is found from the expression

$$\Delta P_{cm} = \frac{2\sigma\cos\theta}{r_c} \quad (2)$$

and the perpendicular and parallel hydrostatic pressure terms are given by

$$\Delta P_n = \rho_l g d_v \cos\psi \quad (3)$$

$$\Delta P_a = \rho_l g L_t \sin\psi \quad (4)$$

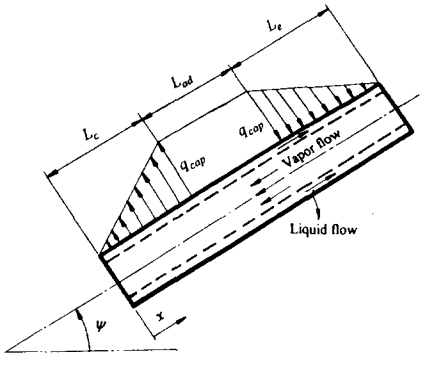

Fig. 1 Schematic illustration of an operating thermosyphon with heat transport q_{cap}

These three terms, shown as the left side of Eq. (1), represent the maximum effective pumping pressure of the wicking structure, or

$$\Delta P_{pm} = \Delta P_{cm} - \Delta P_n - \Delta P_a \quad (5)$$

The liquid frictional coefficient, F_l, was evaluated from the expression

$$F_l = \frac{\mu_l}{K_l A_w \rho_l h_{fg}} \quad (6)$$

$$K_l = \frac{2\varepsilon r_{hl}^2}{f_l Re_l} \quad (7)$$

Similarly, the vapor frictional coefficient, F_v, was evaluated from the expression

$$F_v = \frac{(f_v Re_v)\,\mu_v}{2 r_v^2 A_v \rho_v h_{fg}} \quad (8)$$

To determine the friction factor, f_v, the vapor flow regime must also be evaluated. Expressing the Reynolds number in terms of the heat input, the flow regime was determined from

$$Re_v = \frac{2 r_v q}{A_v \mu_v h_{fg}} \quad (9)$$

For laminar flow, the relationship

$$f_v Re_v = 16 \quad (10)$$

was used, while for turbulent flow the Blasius correlation

$$f_v = \frac{0.079}{Re_v^{0.25}} \quad (11)$$

was used. For the case of the turbulent vapor flow, the vapor friction coefficient was modified by substituting Eq. (11) into (8). This resulted in an expression for the vapor friction coefficient of

$$F_v = \frac{0.039 \mu_v Re_v^{0.75}}{r_v^2 A_v \rho_v h_{fg}} = \frac{0.039 \mu_v}{r_v^2 A_v \rho_v h_{fg}} \left(\frac{2 r_v q}{A_v \mu_v h_{fg}} \right)^{0.75} \quad (12)$$

Substituting this expression and combining with those previously discussed, resulted in a general pressure balance relationship for turbulent vapor flow which takes the form of

$$\Delta P_{pm} = \frac{0.039 \mu_v}{r_v^2 A_v \rho_v h_{fg}} \left(\frac{2 r_v q}{A_v \mu_v h_{fg}} \right)^{0.75} \int_0^{L_t} q^{7/4} dx + F_l \int_0^{L_t} q\, dx \quad (13)$$

Utilizing this expression and a Newton-Raphson method to determine the roots from the resulting

polynomial equation, the maximum heat transport capacity (i.e., capillary limit) for a given heat pipe/thermosyphon of the type under consideration here can be approximated as a function of the evaporator and condenser lengths and operating temperature.

2.2 Viscous limitation

The viscous limit in an operating heat pipe can be approximated utilizing an expression developed by Busse (1973). While it is χ not anticipated that the configuration under investigation here will encounter any problems with the viscous limit, this expression

$$q_{vi}'' = \frac{r_v^2 h_{fg} \rho_v P_v}{16 \mu_v L_{eff}} 5 \tag{14}$$

was used to estimate the power input at which the viscous limit would first occur. Here, P_v is the saturation pressure and L_{eff} is defined as $L_e/2 + L_{ad} + L_c/2$.

2.3 Sonic limitation

Several expressions have been developed by which the sonic limit of operating heat pipe can be approximated. These include a one-dimensional model (Levy, 1968),

$$q_s'' = \rho_o h_{fg} \left(\frac{\gamma_v R_v T_o}{2(\gamma_v + 1)} \right)^{1/2} \tag{15}$$

a similar expression from Chi (1976) using the local vapor temperature and properties instead of the stagnation temperature and properties

$$q_s'' = \rho_v h_{fg} \left(\frac{\gamma_v R_v T_v}{2(\gamma_v + 1)} \right)^{1/2}$$

$$\text{where } R_v = \frac{\bar{R}}{M} \tag{16}$$

and an expression by Busse (1973) which is identical to the above equation if the vapor is assumed to behave as an ideal gas

$$q_s'' = 0.474 h_{fg} (\rho_v P_v)^{1/2} \tag{17}$$

these three expression all yield similar approximations of the maximum heat transport capacity.

2.4 Entrainment limitation

The most common approach to estimating the entrainment in heat pipes is to use the Weber number criterion. This technique compares the ratio of the forces attempting to tear the liquid from the surface (i.e., the shear force) and the forces holding the liquid in the wicking structure (i.e., the surface tension forces). This criterion can be expressed as

$$q_e'' = h_{fg} \left(\frac{\sigma \rho_v}{d_{h,w}} \right)^{1/2} \tag{18}$$

Chi (1976) has proposed that the wick pore diameter, $d_{h,w}$, could be assumed to be equal to the width of the groove for the grooved wicking structure, d_g.

In addition to the Weber number criterion, several different onset velocity criteria have been proposed for use with this expression, These include the critical wavelength criterion by Cotter (1967),

$$U_{vc} = \left(\frac{2\pi\sigma}{\rho_v d_g} \right)^{1/2} \tag{19}$$

which was experimentally verified by Matveev et al. (1977) and Kim et al. (1993). Another criterion was proposed by Rice and Fulford (1987) as

$$U_{vc} = \left(\frac{8\sigma}{\rho_v d_g} \right)^{1/2} \tag{20}$$

Equations (19) and (20) can be converted into expressions for the critical heat transport by combining with the energy balance equation ($q = \rho_v A_v h_{fg} U_v$), which yields

$$q_e'' = \rho_v h_{fg} \left(\frac{2\pi\sigma}{\rho_v d_g} \right)^{1/2} \tag{21}$$

or

$$q_e'' = \rho_v h_{fg} \left(\frac{8\sigma}{\rho_v d_g} \right)^{1/2} \tag{22}$$

respectively, where d_g is the groove width for grooved wicks. However, these criteria may overestimate the entrainment limit if the wick is flooded with liquid. Thus, it is important to note that this criterion can reasonably predict the critical heat transport only if the wick is properly saturated with working fluid (Busse and Kemme, 1980).

Because the current design relies primarily on the angular tilt of the heat pipe to return the liquid from the condenser to the evaporator, a substantial puddle exists along the bottom of the heat pipe. For this reason, it is also necessary to evaluate the entrainment occurring from a free

surface. Estimation of the entrainment limit for a liquid film or free interface can be made by utilizing the inviscid Kelvin-Helmholtz instability theory to determine the critical vapor velocity (Kelvin, 1871; Drazin and Reid, 1981)

$$U_{vc}=\left(\frac{2(\rho_l+\rho_v)}{\rho_l}\right)^{1/2}\left(\frac{\sigma(\rho_l-\rho_v)g}{\rho_v^2}\right)^{1/4} \quad (23)$$

and then using this velocity to estimate the maximum heat transport capacity.

$$q_e''=\rho_v h_{fg} U_{vc}$$
$$=\rho_v h_{fg}\left(\frac{2(\rho_l+\rho_v)}{\rho_l}\right)^{1/2}\left(\frac{\sigma(\rho_l-\rho_v)g}{\rho_v^2}\right)^{1/4} \quad (24)$$

Ishii and Grolmes (1975) also proposed an onset velocity criterion from the roll-wave model for turbulent shear flows and using the critical vapor velocity, an entrainment limit for the flooded wick can be expressed as

$$q_e''=\rho_v h_{fg}\frac{\sigma}{\mu_l}\left(\frac{\rho_l}{\rho_v}\right)^{1/2} N_{vi}^{0.8} \quad (25)$$

$$N_{vi}=\frac{\mu_l}{\left(\rho_l\sigma\sqrt{\frac{\sigma}{\rho_{lv}g}}\right)^{1/2}} \quad (26)$$

2.5 Boiling limitation

In the evaporator section, the liquid at the pipe-wick interface tends to be superheated by an amount depending on not only the fluid and wick properties but also on the heat flux density. In other words, the liquid pressure in the wick is less than the saturation pressure at the liquid-vapor interface by the capillary pressure loss, EMBED Equation ΔP_{cm}(determined by Laplace-Young equation, $\Delta P_{cm}=\sigma(1/r_1+1/r_2)$), caused by the curved liquid interface. Thus, it can be deduced that for the wicked evaporator, nucleate boiling tends to start earlier than for the non-wicked one. Chi (1976) derived the amount of liquid superheat at the onset of the nucleate boiling using a force balance for a spherical bubble near the pipe-wick interface and the Clausius-Clapeyron equation as,

$$T_l-T_v=\frac{T_v}{\rho_v h_{fg}}\left(\frac{2\sigma}{r_n}-\Delta P_{cm}\right) \quad (27)$$

where r_n is the nucleation radius of the vapor bubbles ($2.54\times10^{-7}<r_n<2.54\times10^{-5}$).

However, if thermosyphons or heat pipes operate at a steady state, the wick in the evaporator is no longer flooded with liquid and concave meniscus may be formed in the wick. In this case, the formation of the vapor bubbles in the wick retard the liquid flow and as a result, the evaporator is subjected to an undesirable dry-out. Using the critical liquid super heat in Eq. (27) and the thermal resistance for the liquid-wick annulus, a boiling limit per unit cross-sectional area of the vapor flow was proposed by Chi (1976) as,

$$q_b''=\frac{2\pi L_{eff}k_{eff}T_v}{A_v h_{fg}\rho_v \ln(r_i/r_v)}\left(\frac{2\sigma}{r_n}-\Delta P_{cm}\right) \quad (28)$$

Here, k_{eff} is the effective thermal conductivity of the liquid saturated groove wicks and can be determined by an empirical equation as (Chi, 1976),

$$k_{eff}=\frac{w_f k_l k_w \delta+w k_l(0.185 w_f k_w+\delta k_l)}{(w+w_f)(0.185 w_f k_w+\delta k_l)} \quad (29)$$

where k_l and k_w designate the thermal conductivity of liquid and wick, respectively. Also, w_f represents the groove fin width.

3. Discussions for Transport Limits

The initial approach used in the evaluation of the transport limits was to first use the geometry of the test specimen whose dimensions are listed in Table 1. This test specimen was constructed from a carbon steel pipe approximately 50.8 mm (2 inch) OD with longitudinal axial grooves of the shape illustrated in Fig. 2, running the entire length. The overall length was assumed to be 6.08 m (20 feet) with evaporator and condenser lengths

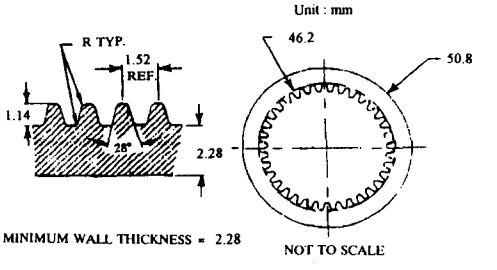

Fig. 2 Configuration of the existing longitudinal wicking structure (from ABB Air Preheater Inc.)

of 3.04 m (10 feet) each. In addition, the heat pipe was assumed to operate at a 7 degree tilt (condenser above the evaporator).

Table 1 Detailed dimensions and wick geometry of the tested thermosyphon

Material	Case	Steel
	Working fluid	Toluene
Diameter	Outer diameter	50.8mm
	Inner diameter	46.2mm
Groove Geometry	Groove depth(δ)	1.14mm
	Groove pitch	1.52mmk
	Groove angle(2α)	28 deg.
Length	Total length(L_t)	6.08m
	Evaporator(L_e)	1.52m
	Condenser(L_c)	1.52m
	Adiabatic section(L_{ad})	3.04m
Orientation	Tilt angle	7 deg.(the evaporator is lower the condenser)

The resulting limits for this configuration, are presented and summarized in Fig. 3 as a function of the vapor temperature. As would be expected in the proposed design, the viscous and sonic limits have very little effect on the maximum transport capacity. However, the capillary, entrainment, and boiling limits all play an important role and must be taken into consideration. As shown in Fig. 3, the capillary limit is relatively constant with respect to the adiabatic vapor temperature. Depending upon the nucleation site radius used in determining the boiling limit, the capillary limit is the governing operating criteria for a significant portion of the operating temperature range. Also as shown, the boiling limit is very sensitive to changes in the nucleation site radius, r_n, with magnitude of the boiling limit varying by as much as factor of ten times for values of r_n ranging from 2.5×10^{-7}m to 2.5×10^{-5}m. An accurate nucleation site radius is extremely difficult to determine and thus, a conservative estimate of 2.5×10^{-5}m should be used.

Another important factor in the estimation of the boiling limit is the maximum capillary pres-

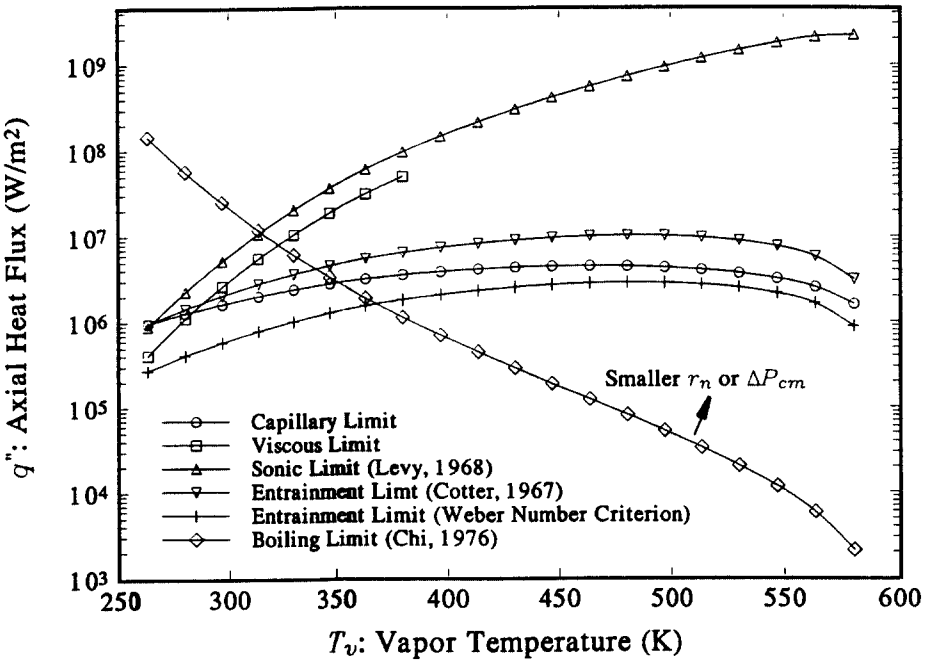

Fig. 3 Performance limits of the tested thermosyphon as a function of the vapor temperature

sure (even though this is relatively smaller than the gravitational hydrostatic head due to the tilt), as indicated in Eq. (28) which shows that the boiling limit heat flux, q_b'', tends to decrease as ΔP_{cm} increases. This implies that any attempt to enhance the capillary limit or ΔP_{pm} in Eq. (5) purely by increasing ΔP_{cm} may cause significant reduction in the boiling limit. In the same manner, the critical liquid superheat in Eq. (27) also tends to decrease with increase in ΔP_{cm}. As a result, the nucleate boiling should initiate at lower liquid superheat. This might be helpful for the successful startup of large scale thermosyphons especially when the evaporator is subjected to possible puddle flow conditions since the nucleate boiling tends to enhance the heat transfer coefficient of the pool boiling (Carey, 1992).

Figure. 4 illustrates the general trends for the entrainment limits of grooved and free interfaces and illustrates that the grooved interfaces show greater limits than those of free interface. This is generally true except for the models proposed by Ishii and Grolmes (1975) and the Weber number criterion in Eqs. (25) and (18), respectively. The roll-wave model of Ishii and Grolmes (1975) seems to be very sensitive to an increase in vapor temperature since only this model takes the effect of liquid viscosity into consideration in addition to the property changes in ρ_v and σ. Equation (25) shows that a large increase in vapor temperature causes both a significant decrease in liquid viscosity and an increase in vapor density, which may result in an over prediction of the entrainment limit. The evaluation of the free surfaces is included herein due to the possible puddle flow conditions existing at low tilt angles.

While comparison of the various transport limitations is helpful in understanding the basic operation, the most important aspect of this analysis is the determination of the relative magnitudes of the individual pressure drop terms and how these magnitudes affect the determination of the maximum effective pumping pressure. The previous analysis indicates that the hydrostatic pressure gain due to the parallel pressure head (i. e., tilt) is several orders of magnitude greater than the capillary pressure due to the axial groove over the entire temperature range. For example, at a temperature of 100℃, the maximum effective pumping pressure, ΔP_{pm} in Eq. (5), is approxi-

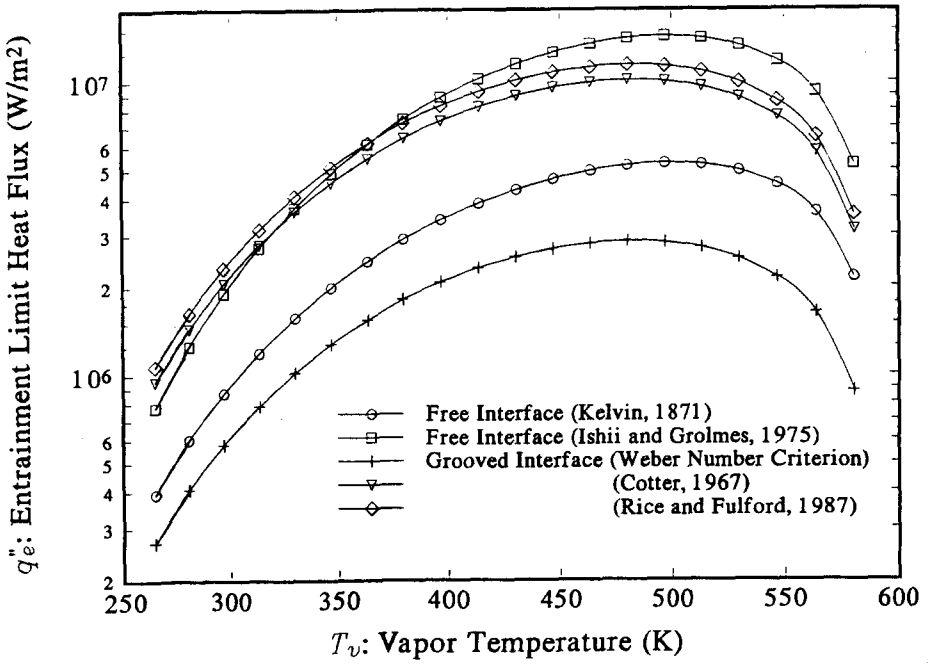

Fig. 4 Comparison of the various entrainment limit models

mately 5394 Pa. The capillary pumping pressure, ΔP_{cm}, resulting from the longitudinal grooves contributes 36 Pa to this total, with the remainder being provided by the hydrostatic pressure caused by the tilt. From this comparison, it is clear that the transport capacity is dominated by the hydrostatic pressure resulting from the tilt and that any variations in the groove size or shape would have little, if any, impact on the capillary transport limitation.

It is important to note that the wicking structure in operating heat pipes serve two distinct functions; first, to provide axial pumping and second, to provide circumferential distribution of the working fluid. The previously described analysis has demonstrated that for the current case the capillary pumping pressure generated by the longitudinal wicking structure is comparatively insignificant. In addition, the longitudinal grooves provide no circumferential distribution of the working fluid and hence, in the current configuration the longitudinal grooves makes almost no contribution to the overall performance of the existing design. It is realized that puddle flow occurring in the bottom region of the thermosyphon is the dominant liquid flow phenomena and that liquid communication with the top grooves is virtually nonexistent.

With regard to the discussion of the capillary limit, if puddle flow does occur, the corresponding result will be for nucleate boiling in the evaporator to occur at even lower levels of heat input. Additionally, with the puddle accumulation in this reflux mode, the end to end temperature difference of the heat pipe will increase due to the added thermal resistance in the heat flow path.

4. Groove Design Optimization

While the longitudinal grooves contribute very little to the overall transport capacity of the heat pipe under evaluation here, it may be possible to develop a configuration which utilizes circumferential grooves to provide distribution of the working fluid. Prior to doing this, it is necessary to optimize the groove shape in order to obtain the maximum capillary pumping pressure and the minimum liquid pressure drop. In doing this, the previous analysis has demonstrated that the several factors must be considered. These include not only the effect of the capillary shape and size on the capillary limit, but also on the entrainment and boiling limits. For this reason, all three limits were evaluated in determining the effect of the groove dimensions on the overall performance limit. The models used in this evaluation include

1. the one dimensional vapor flow model to calculate the capillary limit (Chi, 1976)
2. Cotter's criterion to predict the entrainment limit (Cotter, 1967); and
3. the boiling limit proposed by Chi (1976).

All of the parameters governing these performance limits were represented in terms of the groove dimensions, w, α, w_b, w_f and δ, which are defined in Fig. 5. Several assumptions were made in the evaluation of the groove size and shape. These can be summarized as follows:

1. The liquid meniscus does not recede below the mouth of the groove.
2. $w_b = w_f$(generally $w_f > w_b$ for the convenience of manufacturing). This tends to maximize the liquid flow area if $w_f \geq w_b$ is satisfied.
3. Wetting angle, $\theta = 0$.
4. $T_v = 347$K (165 °F)

Utilizing these assumptions, a numerical computation was performed to examine the effect of the groove angle, α, and the aspect ratio, w/δ, on the performance limitations. For the present computation, the top groove dimension was held

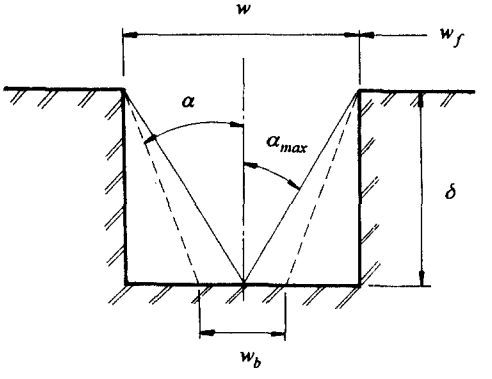

Fig. 5 Basic shape parameters of the grooves

constant at $w=0.04$ inch$=1.016\times10^{-3}$m, while both α and δ were varied, $0\leq\alpha<\alpha_{max}$, $0.05\leq w/\delta\leq4.05$.

The results indicate that the optimal conditions for the groove are those which provide a maximum capillary pumping pressure and a minimal resistance to the liquid flow. Each of the respective terms in the capillary pressure balance and the liquid flow resistance are examined individually, followed by the determination of the maximum heat transport capacity.

4.1 Maximum Capillary Pressure

$$\Delta P_{cm}=\frac{2\sigma\cos\theta}{r_c}\qquad r_c=\frac{w}{\cos\alpha}\tag{30}$$

$\alpha=0$ rectangular groove

$0<\alpha<\alpha_{max}$ trapezoidal

$\alpha=\alpha_{max}$ triangular ($w_b=w_f=0$)

4.2 Liquid Flow Resistance

The permeability of the grooves can be estimated using Eq. (7) and the hydraulic radius of the liquid channel as

$$r_{hl}=\frac{(w+w_b)\,\delta}{\left(\frac{2\delta}{\cos\alpha}+w_b\right)}\tag{31}$$

f_lRe_l for both rectangular and trapezoidal grooves were approximated as:

$$f_lRe_l\left(\frac{w}{\delta}\right)=9.7\left(\frac{w}{\delta}-1\right)^2+14.2\tag{32}$$

For triangular grooves, f_lRe_l was assumed to be 13.3 for all values of w/δ. The liquid flow area could be computed as

$$A_w=F_{aw}\left(\frac{\pi}{4}\right)(d_l^2-d_v^2)\tag{33}$$

where $F_{aw}(=0.5$ for the present study) is the fraction of the liquid area to the total area of the wick annulus. Using Eqs. (31)~(33), the liquid friction coefficient, F_l, can be determined from Eq. (6). To maximize the capillary limit, F_l needs to be minimized, thus, K_lA_w in Eq. (6) should be maximized based on this observation.

In Fig. 6, ΔP_{cm} is presented as a function of α and the aspect ratio. It is evident that the lower aspect ratio has the greater ΔP_{cm}. For the given aspect ratio, ΔP_{cm} tends to decrease with an increase in the groove angle, α. The rate of decrease becomes quite large for large aspect ratios. Figure 7 indicates that the term, K_lA_w, becomes greatest for the aspect ratio, $w/\delta=0.05$

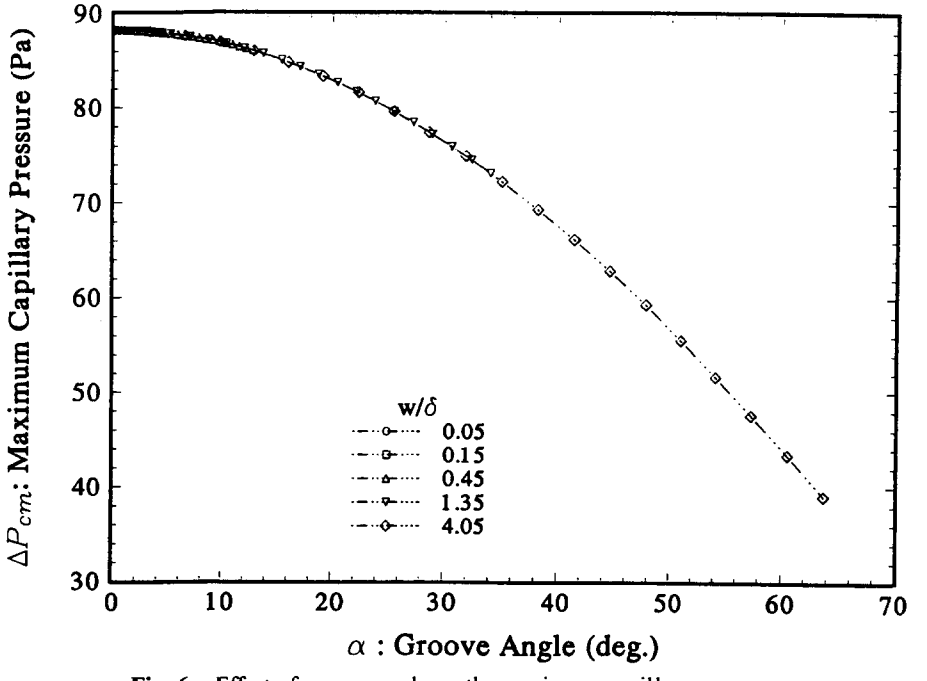

Fig. 6 Effect of groove angle on the maximum capillary pressure

with $\alpha=0$. This implies that a rectangular groove has a greater K_l/A_w value for the same aspect ratio than does a trapezoidal groove. The effect of the groove angle on K_lA_w is significant in the smaller aspect ratios with the effects diminishing as the aspect ratio is increased. The capillary limit

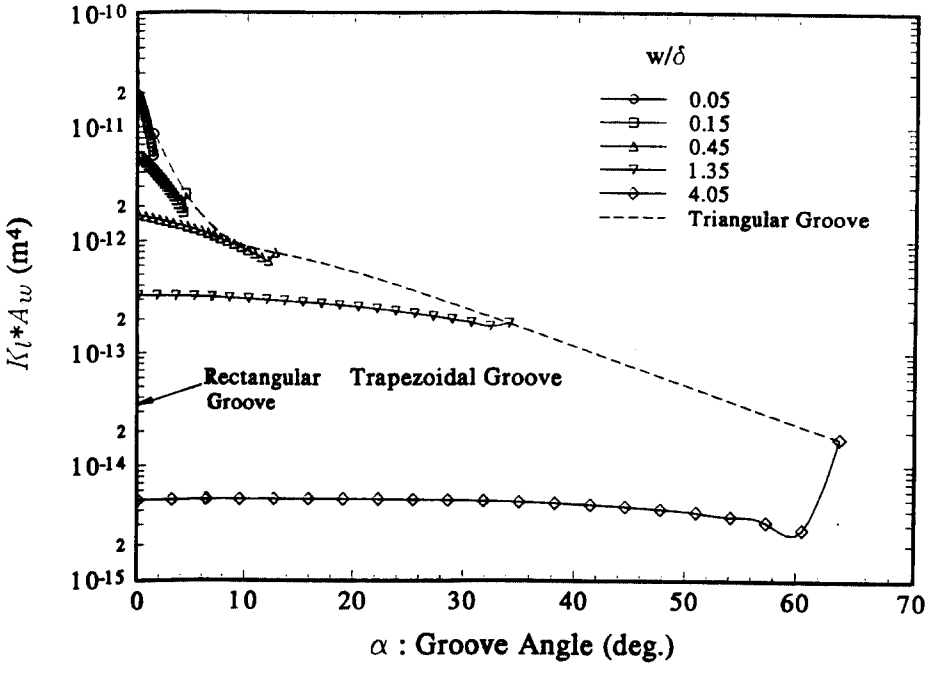

Fig. 7 Effect of groove angle on the permeability of the grooves for various aspect ratios

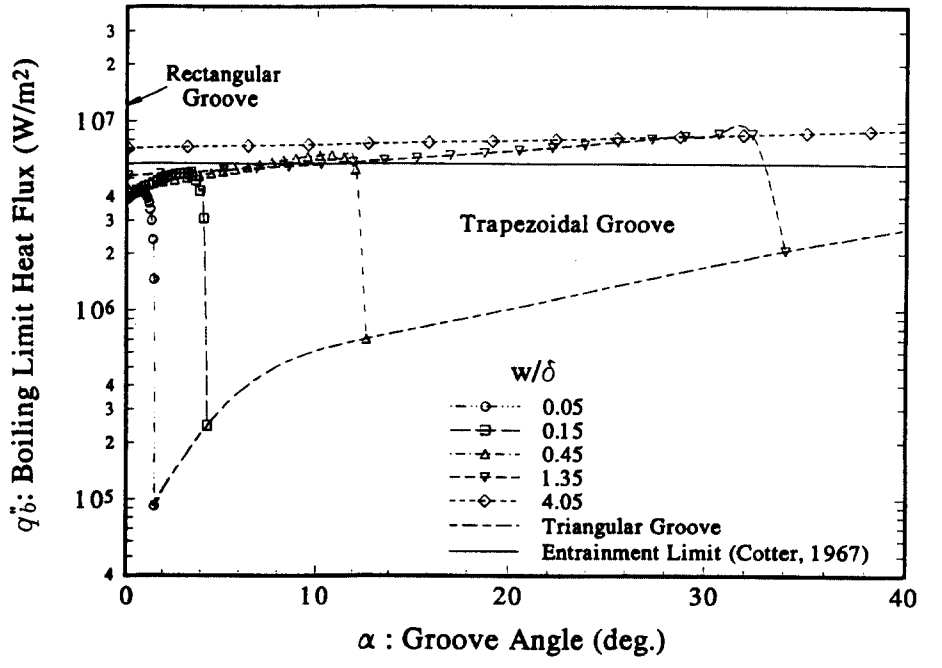

Fig. 8 Effect of groove angle on the boiling limit heat flux for different aspect ratios

exhibited the same trends as the $K_l A_w$ term presented in Fig. 7.

Figure 8 presents the boiling limit as a function of groove angle for various aspect ratios. It is evident that the boiling limit is very sensitive for small aspect ratios ($w/\delta < 1.35$). However, the boiling limit becomes less sensitive to the groove angle for larger aspect ratios ($w/\delta \geq 1.35$).

In summary, the ideal groove shape for the application under consideration here is that of a rectangular groove whose aspect ratio is as small as possible yet still has the capability of wicking to a height slightly larger than the diameter of the heat pipe. This groove, however, may present problems from the standpoint of manufacturing. Also, it may cause a significant decrease of the boiling limit when the groove width is very small. For this reason, the groove width should be as large as possible to allow for increases in the superheat required for the onset of nucleate boiling. However, as mentioned earlier, the large groove width (e.g. $w/\delta \geq 4.05$) may cause problems in the startup since lower tion ΔP_{cm} retard initiation of the nucleate boiling. Consequently, the aspect ratio, w/δ, must be optimized from this standpoint.

A second approach to enhancing performance is to use the intermediate aspect ratio ($1 \sim 1.35$) to avoid a drastic decrease in the boiling limit caused by the small size of the grooves. While this approach would slightly decrease in the capillary pumping pressure it would provide a means by which any bubbles forming in the grooves could be vented. Care should be taken to maintain an aspect ratio of less than 1.35 since as illustrated in Fig. 8, significant decrease in the heat flux may result at which boiling occurs.

5. Conclusions

Based upon the results discussed in the GROOVE DESIGN OPTIMIZATION, it is recommended that the groove design be altered. The groove design should be modified by replacing (or adding to) the longitudinal grooves in the initial design stage with circumferential grooves to provide even distribution of the working fluid over the entire evaporator surface and to decrease the size of the puddle formed in the bottom of the pipe. These circumferential grooves may be in the form of spiral, knurled, or pure circumferential grooves.

The aspect ratio and the groove angle turned out to be the most important factors in optimizing the configuration of grooves. As indicated in Fig. 7 and 8, $K_l A_w$ and q_b'' tend to be significantly degraded if the aspect ratio, w/δ, is less than unity. Hence, in order to optimize $K_l A_w$ and q_b'' and to avoid entrainment possible in the case of the large aspect ratio (e.g., $w/\delta = 4.05$), the aspect ratio should be between 1 and 1.35 and the groove angle (α) less than 15 degree is preferred, as indicated in Fig. 8. Thus, the groove width (w) should be in the range of 1.1 mm to 1.5 mm for the given groove depth ($\delta = 1.14$ mm in the present study). These dimensions and shape would provide the necessary circumferential pumping capacity while still maximizing the boiling and entrainment limits.

References

Busse, C. A., 1973, "Theory of the Ultimate Heat Transfer Limit of Cylindrical Heat Pipes," *International Journal of Heat Mass Transfer*, Vol. 16, p. 169.

Busse, C. A. and Kemme, J. E., 1980, "Dry-out Phenomena in Gravity-Assisted Heat Pipes with Capillary Flow," *International Journal of Heat Mass Transfer*, Vol. 23, pp. 634~654.

Carey, V. P., 1992, *Liquid-Vapor Phase Change Phenomena*, Hemisphere Publishing Co., Washington, D. C., pp. 90~98, 229~331.

Chi, S. W., 1976, *Heat Pipe Theory and Practice*, Hemisphere Publishing Co., Washington, D. C., pp. 33~95.

Cotter, T. P., 1967, "Heat Pipe Startup Dynamics," *Proceedings of the SAE Thermionic Conversion Specialist Conference*, Palo Alto, California, October, pp. 344~347.

Drazin, P. G. and Reid, W. H., 1981, *Hydrodynamic Stability*, Cambridge University Press, Cambridge, United Kingdom, pp. 14~22.

Dunn, P. D. and Reay, D. A., 1982, *Heat Pipes*,

Pergamon Press, Oxford, United Kingdom, pp. 23 ~85, 138~172.

Ishii, M. and Grolmes, M.A., 1975, "Inception Criteria for Droplet Entrainment in Two-Phase Concurrent Film Flow," *AIChE J.*, Vol. 21, pp. 308~318.

Ivanovskii, M. N., Sorokin, V. P. and Yagodkin, I. V., 1982, *The Physical Principles of Heat Pipe*, Clarendon Press, Oxford, United Kingdom, pp. 107~115.

Kelvin, Lord, 1871, "Hydrokinetic solutions and observations," *Phil. Mag.*, Vol. 10, pp. 155 ~168.

Kim, B. H., Peterson, G. P. and Kihm, K. D., 1993, "Analytical and Experimental Investigation of Entrainment in Capillary-Pumped Wicking Structures," *Transactions of the ASME J. of Energy Resources and Technology*, Vol. 115, pp. 278~286.

Levy, E. K., 1968, "Theoretical Investigation of Heat Pipes Operating at Low vapor Pressure," *J. of Eng. Ind.*, Vol. 90, pp. 547~552.

Matveev, V. M., Filippov, Y. N., Dyuzhev, V. I. and Okhapkin, E. V., 1977, "Breakaway of a Liquid by a Gas Stream at an Interface Containing Grid," *Journal of Engineering Physics*, Vol. 33, No. 3, pp. 1008~1012.

Peterson, G. P. and Bage, B., 1991, "Entrainment Limitations in Thermosyphons and Heat Pipes," *ASME J. of Energy Resources Technology*, Vol. 113, No. 3, pp. 147~154.

Prenger, F. C. and Kemme, J. E., 1981, "Performance Limits of Gravity-Assisted Heat Pipes with Simple Wick Structures," *Proceedings of The 4th International Heat Pipe Conference*, London, United Kingdom, September, pp. 137~146.

Rice, G. and Fulford, D., 1987, "Influence of a Fine Mesh Screen on Entrainment in Heat Pipes," *Proceedings of The 6th International Heat Pipe Conference*, Grenoble, France, May, pp. 168 ~172.

Tien, C. L. and Chung, K. S., 1979, "Entrainment Limits in Heat Pipes," *AIAA Journal*, Vol. 17, No. 6, pp. 230~238.